Experimental and Theoretical Analysis of Composite I-Beams with Elastic Couplings

Ramesh Chandra* and Inderjit Chopra†
University of Maryland, College Park, Maryland 20742

This paper presents a theoretical-cum-experimental study on the static structural response of composite I-beams with elastic couplings. A Vlasov-type linear theory is developed to analyze composite open section beams made out of general composite laminates, where the transverse shear deformation of the beam cross section is included. In order to validate this analysis, graphite-epoxy and Kevlar-epoxy symmetric I-beams were fabricated using an autoclave molding technique. The beams were tested under tip bending and torsional loads, and their structural response in terms of bending slope and twist was measured with a laser optical system. Good correlation between theoretical and experimental results is achieved. A 630% increase in the torsional stiffness due to constrained warping is noticed for graphite-epoxy beams with slenderness ratio of 30. Also extension-twist coupling "B_{16}" of flanges of these I-beams increases the bending-torsion coupling stiffness of beams manyfold.

Nomenclature

$2b$, $2h$	= width and height of I-beam
E_1, E_2	= Young's moduli in principal directions of plies of beam
G_{12}	= shear modulus of plies in principal plane
K_{ij}	= stiffness matrix for beam
k_s, k_z, k_{sz}	= bending curvatures referring to plate segment
l	= length of I-beam
M_s, M_z, M_{sz}	= moment resultants referring to plate segment
M_x, M_y	= bending moments referring to beam
M_ω	= bimoment (or warping moment) referring to beam
N	= axial force referring to beam
N_s, N_z, N_{sz}	= stress resultants referring to plate segment
n, s, z	= coordinate system for plate segment, Fig. 1b
P	= applied force at tip of beam
T	= torsion moment referring to beam
$\bar{T}$	= applied torsion at tip of beam
U, V, W	= displacements in x, y, z directions, referring to beam
u, v, w	= displacements in n, s, z directions, referring to plate segment
V_x, V_y	= shear forces in x, y directions, referring to beam
x, y, z	= coordinate system for I-beam, Fig. 1a
ε_s, ε_z, ε_{sz}	= membrane strains referring to plate segment
ε_{xz}, ε_{yz}	= transverse shear strains for the beam in xz and yz planes, respectively
μ	= constrained warping parameter
μ_{12}	= Poisson's ratio of plies in principal plane
σ_s, σ_z, σ_{sz}	= stress field referring to plate segment
φ	= warping function
ϕ_x, ϕ_y, ϕ_z	= rotations about x, y, z axes, referring to beam
$(\ )'$	= differentiation with respect to z coordinates of beam
$(\ )^{(b)}$	= bottom flange of I-beam
$(\ )^{(t)}$	= top flange of I-beam
$(\ )^{(w)}$	= web of I-beam

Received Feb. 4, 1991; presented as Paper 91-1024 at the AIAA/AHS/ASME/ASCE/ASC 32nd Structures, Structural Dynamics and Materials Conference, Baltimore, MD, April 8–10, 1991; revision received June 6, 1991; accepted for publication June 6, 1991.

*Research Associate, Department of Aerospace Engineering. Member AIAA.
†Professor, Department of Aerospace Engineering. Fellow AIAA.

Introduction

THIN-WALLED composite beams with closed and open cross sections are widely used in aerospace structures, in particular in the construction of helicopter rotor blades. Through the control of lamination parameters (i.e., ply orientation and stacking sequence), such structural couplings, as bending-twisting and extension-twisting, are introduced. Traditionally, the necessary couplings used in helicopter rotors, such as pitch-flap and pitch-lag, are introduced by mechanical means. Past studies[1,2] have shown that elastic couplings due to composites have strong influence on blade dynamic characteristics, including aeroelastic stability, vibration, dynamic stresses, and loads. Beams are categorized as symmetric and antisymmetric based on their lay-ups. In a symmetric configuration, the ply lay-ups on opposite flanges are symmetric with respect to the mid-axis of the section, whereas for an antisymmetric configuration, the ply lay-ups on opposite flanges are of reversed orientation. The symmetric configurations result in bending-twist and extension-shear couplings, whereas antisymmetric-configuration beams experience extension-twist and bending-shear couplings.

In order to validate the simple structural model employed in the above mentioned aeroelastic analyses, thin-walled composite box beams with bending-twist and extension-twist couplings were fabricated out of graphite-epoxy plies using an autoclave molding technique.[3] The experimental values of bending slope and twist under bending, torsional and extensional loads, measured by using a laser optical system, were compared with theoretical values. The correlation was satisfactory for extension-twist coupled beams; however for bending-twist coupled beams, the correlation was less satisfactory. This showed the need to improve the modeling of composite thin-walled beams. Consequently, in a subsequent study,[4] the structural modeling was modified where warping, transverse shear, and appropriate representation of inplane elasticity were included. This modified structural model improved the correlation with experimental data for several different composite beams. Experimental and analytical studies on the vibration characteristics of thin-walled composite box beams under rotating conditions were carried out in Ref. 5. For this, a specialized facility, a 10-ft-diam vacuum chamber, was used to test rotor models in the absence of aerodynamic forces. The natural frequencies and mode shapes of the composite box beam were correlated successfully with the theoretical values obtained using Galerkin's method (continuum approach). Again, this showed the importance of nonclassical effects such as section warping and transverse shear on the free vibration characteristics of composite beams. There are other investigations on closed cross section beams ranging from simple analytical models[6–9] to detailed finite element models.[10–12] Thus a better understanding of thin-walled closed-section composite beams under static and dynamic loads than of open-section composite beams is seen.

Such open-section composite beams as I-beams are used in the fabrication of flex beams (root end) of a bearingless rotor. Hong and Chopra[13] showed that bending-twist and extension-twist couplings introduced through ply orientations in I-beams influenced the blade dynamics of bearingless rotors significantly. The structural model used in that study was based on the solid section approach; constrained warping and transverse shear effects were not considered. Rehfield and Atilgan[14] presented a buckling analysis of composite open-section beams. The wall thickness of the beam was assumed to be thin enough to neglect its bending stiffness, but the transverse shear deformation of the beam cross section was accounted for.

Development of beam theory (open as well as closed section) essentially addresses the reduction of two- or three-dimensional stress and displacement fields to one-dimensional generalized force and displacement fields. Vlasov[15] and Gjelsvik[16] presented an isotropic beam theory wherein two-dimensional stress and displacement fields were identified with those of plate or shell segments of the beam. The plate/shell displacements were related to the generalized beam displacements through geometric considerations, whereas the plate/shell stresses were connected to the generalized beam forces via the virtual work principle. Bauld and Tzeng[17] extended Vlasov's theory to open-section beams made out of midplane symmetric composite laminates.

In the present investigation, Vlasov's theory is expanded to analyze open sections like I-beams made out of general composite laminates in which transverse shear effects are also included. In order to provide experimental correlation of the analysis, graphite-epoxy I-beams of five different configurations were fabricated using an autoclave molding technique. These beams were cantilevered and tested under bending and torsional loads, and their static structural response in terms of bending slope and twist was measured using a laser optical system. To simulate the boundary conditions of the beams in the experiment, theoretical results are obtained for constrained warping at clamped and loading edges. The adequacy of modeling is checked from the comparison of predicted and measured results.

Analysis

The present theory uses three coordinate systems: an orthogonal Cartesian coordinate system (x, y, z) for the beam (Fig. 1a); an orthogonal coordinate system (n, s, z), for any plate segment of the beam (Fig. 1b), where the n axis is normal to the midsurface of any plate segment, the s axis is tangential to the midsurface and is along the contour line of the beam cross section, and the z axis is along the longitudinal axis of beam; and a contour coordinate system s, where s is measured along the contour line of the cross section from a judiciously selected origin (Fig. 1c). The seven generalized bar forces V_x, V_y, V_z, M_x, M_y, T, and M_ω are shown in Fig. 1b. The torsional moment T consists of unconstrained warping torsion (Saint Venant torsion), and constrained warping torsion (Vlasov torsion). As shown later, the Vlasov torsion and bimoment M_ω are related to each other. The stress resultants, moment resultants, and transverse shear forces acting on any general plate segment of beam are shown in Fig. 1b. The plate stress and displacement fields are functions of s and z.

The essence of this theory is the reduction of two-dimensional stress and displacement fields to one-dimensional beam forces and displacements.

Fundamental Assumptions

Three basic assumptions used in the present theory are:

1) The contour (midline of the plate segments) of a cross section does not deform in its plane. This means that the inplane warping of the cross section is neglected and the normal strain ε_s in the contour direction is neglected in comparison with the normal axial strain ε_z. This assumption was introduced by Vlasov.[15]

2) The normal stress σ_s is neglected in comparison with σ_z.

3) Any general plate segment of the beam behaves as a thin plate. This implies that the transverse shear deformation of the plate segment is not accounted for, although the transverse shear deformation of the beam is considered.

These assumptions imply that the nonzero membrane strains and bending curvatures for the plate segment are ε_z, ε_{sz}, k_z, and k_{sz}. An additional assumption due to layered composite material of the beam is:

4) A general plate segment of the beam is governed by linear classical laminated plate theory.

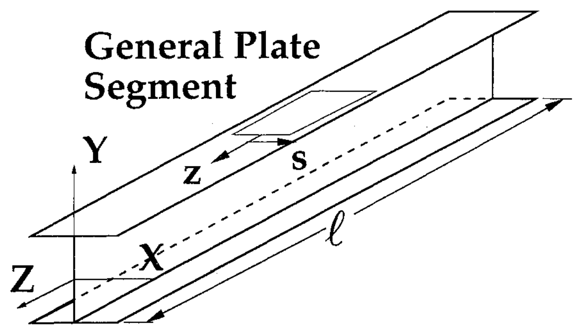

Fig. 1a Coordinates in I-beam.

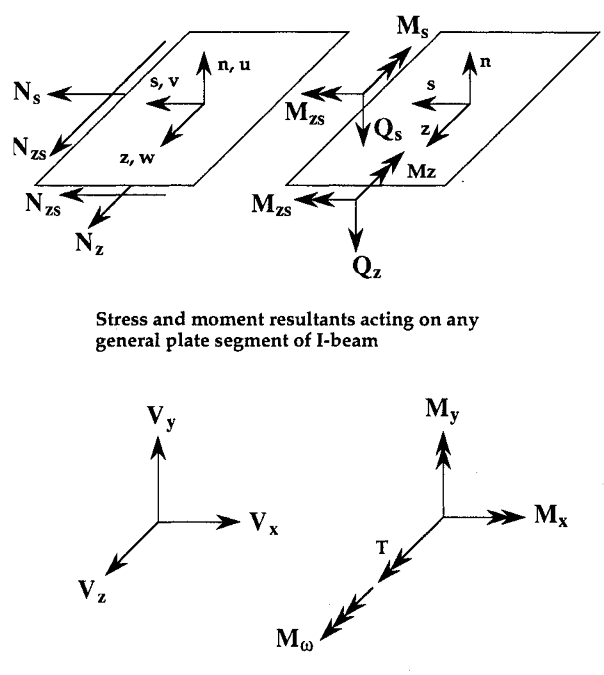

Fig. 1b Bar forces and plate forces.

Kinematics

From geometric considerations (Fig. 1c), the plate displacements $u(z, s)$ and $v(z, s)$ are related to the beam displacements U, V, and ϕ_z as

$$u(z, s) = U(z)\sin\theta(s) - V(z)\cos\theta(s) - q(s)\phi_z(z) \quad (1)$$

$$v(z, s) = U(z)\cos\theta(s) + V(z)\sin\theta(s) + r(s)\phi_z(z) \quad (2)$$

where r, q, and θ are shown in Fig. 1c.

The axial displacement $w(z, s)$ is determined from the following shear strain-displacement relation:

$$\varepsilon_{zs} = w_{,s} + v_{,z} \quad (3)$$

Vlasov made another geometric assumption that states that the shear strain ε_{zs} is negligible and therefore is set to zero. However, in the present analysis the shear strain is nonzero due to transverse shear deformation of the beam. Again, from geometric considerations and strain transformation law

$$\varepsilon_{zs} = \varepsilon_{xz}\cos\theta + \varepsilon_{yz}\sin\theta \quad (4)$$

Using relations (3) and (4), $w(z, s)$ is obtained as

$$w(z, s) = W + x\phi_x + y\phi_y - \varphi\phi_z' \quad (5)$$

where φ is a warping function and is expressed in terms of sectorial area

$$\varphi = \int_s r\,\mathrm{d}s$$

$$\phi_x = \varepsilon_{xz} - U'$$

$$\phi_y = \varepsilon_{yz} - V' \quad (6)$$

Plate strain ε_z is related by the following equation:

$$\varepsilon_z = w_{,z} \quad (7)$$

Using relations (5) and (7), ε_z is obtained as

$$\varepsilon_z = W' + x\phi_x' + y\phi_y' - \varphi\phi_z'' \quad (8)$$

Similarly k_z and k_{zs} are obtained as

$$k_z = -\sin\theta\phi_x' + \cos\theta\phi_y' - q\phi_z'' + \varepsilon_{xz}'\sin\theta - \varepsilon_{yz}'\cos\theta \quad (9)$$

$$k_{zs} = -2\phi_z' \quad (10)$$

Thus the nonzero membrane strains and bending curvatures in the plate segment are given by relations (8), (4), (9), and (10).

Plate Stress Field

Using classical laminated plate theory, the stress resultants and moment resultants are

$$N_z = A_{11}\varepsilon_z + A_{16}\varepsilon_{zs} + B_{11}k_z + B_{16}k_{zs}$$

$$N_{zs} = A_{16}\varepsilon_z + A_{66}\varepsilon_{zs} + B_{16}k_z + B_{66}k_{zs}$$

$$M_z = B_{11}\varepsilon_z + B_{16}\varepsilon_{zs} + D_{11}k_z + D_{16}k_{zs}$$

$$M_{zs} = B_{16}\varepsilon_z + B_{66}\varepsilon_{zs} + D_{16}k_z + D_{66}k_{zs} \quad (11)$$

where $[A]$, $[B]$, and $[D]$ are defined in the Appendix.

Here, the flanges and web of I-beams are treated as general composite laminates. It is to be noted that Bauld and Tzeng[17] considered these as symmetric with respect to their midsurfaces (in-plane-bending coupling stiffness matrix $[B]$ was neglected), whereas Rehfield and Atilgan[14] neglected the bending stiffnesses of these segments. This means that only membrane behavior was captured in Ref. 6.

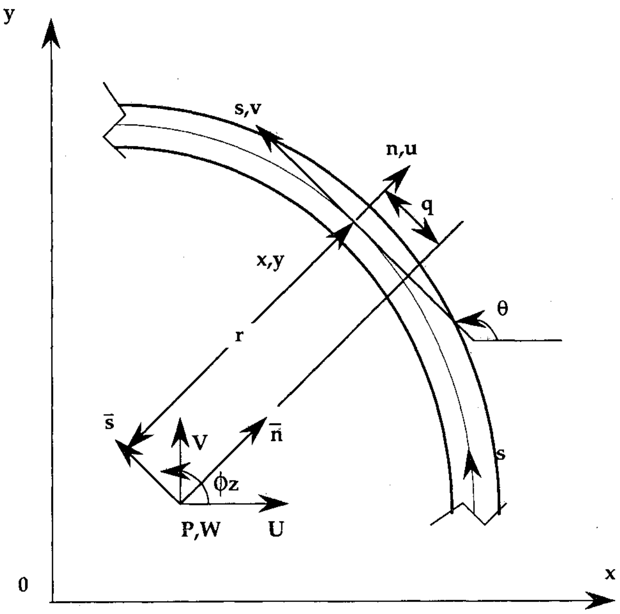

Fig. 1c Pictorial definitions of beam displacements and rotation.

Bar Forces and Their Equilibrium Equations

The generalized forces of bar and their equilibrium equations are derived by applying the principle of virtual work. This approach is similar to the one used by Gjelsvik[16] except the transverse shear deformation of the bar was not taken into account. The external work done by the shell/plate forces during a displacement of the cross section is

$$W_e = \int_s [N_z w + M_z u' + N_{zs} v - Q_z u - M_{zs}\phi_z]\,\mathrm{d}s + \sum_{\text{branches}} (M_{zs}^j u^j - M_{zs}^i u^i) \quad (12)$$

Using relations (1), (2), and (5) and taking the variation of W_e

$$\delta W_e = N\delta W + V_x\delta U + V_y\delta V + T\delta\phi_z + M_\omega\delta\phi_z' + M_y\delta\phi_x + M_x\delta\phi_y + F_x\delta\varepsilon_{xz} + F_y\delta\varepsilon_{yz} \quad (13)$$

where

$$N = \int_s N_z\,\mathrm{d}s \quad (14)$$

$$V_x = \int_s (N_{zs}\cos\theta - Q_z\sin\theta)\,\mathrm{d}s + \sum_{\text{branches}} (M_{zs}^j\sin\theta^j - M_{zs}^i\sin\theta^i) \quad (15)$$

$$V_y = \int_s (N_{zs}\sin\theta + Q_z\cos\theta)\,\mathrm{d}s + \sum_{\text{branches}} (-M_{zs}^j\sin\theta^j + M_{zs}^i\sin\theta^i) \quad (16)$$

$$T = \int_s (N_{zs}r + Q_z q - M_{zs})\,\mathrm{d}s + \sum_{\text{branches}} (-M_{zs}^j q^j + M_{zs}^i q^i) \quad (17)$$

$$M_\omega = -\int_s (N_z\varphi + M_z q)\,\mathrm{d}s \quad (18)$$

$$M_x = \int_s (N_z y + M_z \cos\theta)\, ds \tag{19}$$

$$M_y = \int_s (N_z x - M_z \sin\theta)\, ds \tag{20}$$

$$F_x = \int_s M_z \sin\theta\, ds \tag{21}$$

$$F_y = -\int_s M_z \cos\theta\, ds \tag{22}$$

It is difficult to compute the generalized bar forces V_x, V_y, and T from relations (15), (16), and (17) because of the contributions from different branches. These are simplified by using equilibrium equations of plate/shell forces[16]:

$$V_x = -M_y' \tag{23}$$

$$V_y = M_x' \tag{24}$$

$$T = T_s + T_\omega \tag{25}$$

where T_s is Saint Venant torsion (free warping) and T_ω is Vlasov torsion (constrained warping). These are defined as

$$T_s = -2\int_s M_{zs}\, ds \tag{26}$$

$$T_\omega = \int_s (N_{zs} r + M_z' q)\, ds \tag{27}$$

By using the plate/shell equilibrium equation, relation (27) is simplified to

$$T_\omega = -M_\omega' \tag{28}$$

This gives the relationship between Vlasov torsion and warping moment (or bimoment). The external virtual work done by the applied loadings on the shell/plate is

$$p\delta W + v_x\delta U + v_y\delta V + t\delta\phi_z + m_\omega\delta\phi_z'' + m_y\delta\phi_x + m_x\delta\phi_y + f_x\delta\varepsilon_{xz} + f_y\delta\varepsilon_{yz} \tag{29}$$

where p, v_x, v_y, t, m_ω, m_y, m_x, f_x, and f_y are generalized load intensities on the beam, derived from the loadings on shell.[16]

The strain energy Π is given as

$$\Pi = \frac{1}{2}\int_s (N_z\varepsilon_z + N_{zs}\varepsilon_{zs} + M_z k_z + M_{zs}k_{zs})\, ds \tag{30}$$

Using the relations between bar forces and shell forces, the strain energy becomes

$$\Pi = \tfrac{1}{2}[NW' + M_y\phi_x' + M_x\phi_y' + T\phi_z' + M_\omega\phi_z'' + F_x\varepsilon_{xz}' + F_y\varepsilon_{yz}' + G_x\varepsilon_{xz} + G_y\varepsilon_{yz}] \tag{31}$$

The internal virtual work W_i is obtained from the strain energy as

$$-W_i = NW' + M_y\phi_x' + M_x\phi_y' + T\phi_z' + M_\omega\phi_z'' + F_x\varepsilon_{xz}' + F_y\varepsilon_{yz}' + G_x\varepsilon_{xz} + G_y\varepsilon_{yz} \tag{32}$$

where

$$G_x = \int_s N_{zs}\cos\theta\, ds \tag{33}$$

$$G_y = \int_s N_{zs}\sin\theta\, ds \tag{34}$$

Equilibrium equations for bar forces are obtained by considering a bar element and equating the external work to internal work for any virtual displacement. Thus these equations are

$$V_x' + v_x = 0 \tag{35}$$

$$V_y' + v_y = 0 \tag{36}$$

$$N' + n = 0 \tag{37}$$

$$T' + t = 0 \tag{38}$$

$$M_\omega' + T - T_s + m_\omega = 0 \tag{39}$$

$$M_y' + V_x + m_y = 0 \tag{40}$$

$$M_x' - V_y + m_x = 0 \tag{41}$$

$$F_x' - G_x + f_x = 0 \tag{42}$$

$$F_y' - G_y + f_y = 0 \tag{43}$$

By eliminating V_x, V_y, and T, the equations are reduced to six equations:

$$N' + n = 0 \tag{44}$$

$$M_y'' + m_y' - v_x = 0 \tag{45}$$

$$M_x'' + m_x' + v_y = 0 \tag{46}$$

$$M_\omega'' - T_s' + m_\omega' - t = 0 \tag{47}$$

$$F_x' - G_x + f_x = 0 \tag{48}$$

$$F_y' - G_y + f_y = 0 \tag{49}$$

Bar Forces–Displacement Relations

There are nine generalized bar forces, namely N, M_y, M_x, M_ω, T_s, F_x, F_y, G_x, and G_y, appearing in the above equations. These nine generalized bar forces are related to six generalized displacements. Using plate stress-strain relations (11) and plate strain-beam displacement relations (8), (4), (9), and (10), the relations between the generalized bar forces and displacements for a general case are obtained (see Ref. 18).

Symmetric I-Beams Under Bending and Torsional Loads

For I-beams with identical flanges and orthotropic webs (the coefficients A_{16}, A_{26}, D_{16}, and D_{26} of $[A]$ and $[D]$ matrices are zero), the force-displacement relations are simplifed to

$$\begin{bmatrix} N \\ G_x \\ G_y \end{bmatrix} = \begin{bmatrix} K_{11} & K_{16} & K_{17} \\ K_{16} & K_{66} & 0 \\ K_{17} & 0 & K_{77} \end{bmatrix} \begin{bmatrix} W' \\ \varepsilon_{xz} \\ \varepsilon_{yz} \end{bmatrix} \tag{50}$$

$$\begin{bmatrix} M_x \\ -M_y \\ M_\omega \\ T_s \\ F_x \\ F_y \end{bmatrix} = \begin{bmatrix} K_{22} & 0 & 0 & K_{25} & 0 & 0 & 0 & K_{29} \\ 0 & K_{33} & 0 & 0 & 0 & 0 & K_{38} & 0 \\ 0 & 0 & K_{44} & 0 & 0 & 0 & 0 & 0 \\ K_{25} & 0 & 0 & K_{55} & 0 & 0 & 0 & K_{59} \\ 0 & K_{38} & 0 & 0 & 0 & 0 & K_{88} & 0 \\ 0 & K_{29} & 0 & 0 & K_{59} & 0 & 0 & K_{99} \end{bmatrix} \begin{bmatrix} \phi_y' \\ \phi_x' \\ \phi_z'' \\ \phi_z' \\ \varepsilon_{xz}' \\ \varepsilon_{yz}' \end{bmatrix} \tag{51}$$

where K_{ij} coefficients are given in the Appendix. It is to be noted that the symmetric beams have extension-shear and bending-twist couplings. From relation (51)

Bending:

$$M_x = K_{22}\phi_y' + K_{25}\phi_z' + K_{29}\varepsilon_{yz}' \tag{52}$$

Torsion:

$$T_s = K_{25}\phi_y' + K_{55}\phi_z' + K_{59}\varepsilon_{yz}' \tag{53}$$

Using relation (6), these equations become

$$M_x = K_{22}(\varepsilon_{yz}' - V'') + K_{25}\phi_z' + K_{29}\varepsilon_{yz}' \tag{54}$$

$$T_s = K_{25}(\varepsilon_{yz}' - V'') + K_{55}\phi_z' + K_{59}\varepsilon_{yz}' \tag{55}$$

ε_{yz} is obtained by inverting Eq. (50) as

$$\varepsilon_{yz} = L_{17}N + L_{77}G_y \tag{56}$$

where $[L] = [K]^{-1}$, $[K]$ is given in Eq. (50).

For a bar subjected to bending or torsional loads at the tip, $\varepsilon_{yz}' = 0$. Hence Eqs. (54) and (55) are reduced to

$$M_x = -K_{22}V'' + K_{25}\phi_z' \tag{57}$$

$$T_s = -K_{25}V'' + K_{55}\phi_z' \tag{58}$$

It is important to note that the transverse shear does not influence the bending and torsional behavior of these beams under tip loadings. However, it will influence the behavior for loadings that result in nonzero ε_{yz}'. Including the contribution of constrained warping on torsion from relation (28) via M_ω, Eq. (58) is modified to

$$T = -K_{44}\phi_z''' + K_{55}\phi_z' - K_{25}V'' \tag{59}$$

The bending and torsional behavior of the symmetric I-beams is governed by Eqs. (57) and (59). These equations are solved for cantilever beams as follows.

Tip torsional load:

$$M_x = 0; \qquad T = \bar{T} \tag{60}$$

Equations (57) and (59) are combined to give

$$K_{44}\phi''' - (K_{55})_r\phi_z' = -\bar{T} \tag{61}$$

where $(K_{55})_r = K_{55} - (K_{25}^2/K_{22})$.

The general solution of Eq. (61) is

$$\phi_z = \left[\frac{\bar{T}}{(K_{55})_r}\right] z + A + B\sinh\lambda z + C\cosh\lambda z \tag{62}$$

where

$$\lambda^2 = (K_{55})_r/K_{44} \tag{63}$$

The arbitrary constants involved in the solution are determined using the boundary conditions. The boundary conditions associated with bending are well known. Gjelsvik[16] gives a good account of various boundary conditions associated with torsion. It is worth recapitulating here that ϕ_z' is zero at a boundary where warping deformation is restrained. At this boundary, the Saint Venant torsion is zero and the total torsion transmitted to the support is the constrained warping torsion. At a boundary where warping is permitted, M_ω and therefore ϕ_z'' is zero.

Because the present analysis is compared with experiment, the boundary conditions simulated in the experiment are considered. Constrained warping is considered at both the boundaries, clamped and loading ends. These are as follows.

Clamped end:

$$\phi_z(z=0) = 0; \qquad \phi_z'(z=0) = 0; \qquad V'(z=0) = 0 \tag{64}$$

Loading end:

$$\phi_z'(z=l) = 0$$

These refer to the constrained warping at clamped and loading ends.

The expressions for twist and induced bending slope are

$$\phi_z = \frac{\bar{T}}{\lambda(K_{55})_r} \times \left[\lambda z - \sinh\lambda z + \frac{\cosh\mu - 1}{\sinh\mu}(\cosh\lambda z - 1)\right] \tag{65}$$

$$\phi_y = \frac{K_{25}}{K_{22}}\frac{\bar{T}}{(K_{55})_r}\frac{1}{\lambda} \times \left[\lambda z - \sinh\lambda z + \frac{\cosh\mu - 1}{\sinh\mu}\cosh\lambda z\right] \tag{66}$$

where

$$\mu = \lambda l = \sqrt{\frac{(K_{55})_r}{K_{44}}}\, l \tag{67}$$

Tip Bending Load:

$$M_x = P(z - l); \qquad T = 0 \tag{68}$$

Equations (57) and (59) are solved for the above loading and the arbitrary constants are evaluated by using the boundary conditions given by relation (64). Thus the bending slope and induced twist are

$$\phi_y = \frac{P}{2K_{22}^2}\left(K_{22} + \frac{K_{25}^2}{(K_{55})_r}\right)(z^2 - 2lz) - \frac{K_{25}^2}{K_{22}^2}\frac{Pl}{\lambda(K_{55})_r}[\coth\mu(\cosh\lambda z - 1) - \sinh\lambda z] \tag{69}$$

$$\phi_z = \frac{K_{25}}{K_{22}}\frac{Pl}{\lambda(K_{55})_r} \times \left[\coth\mu(\cosh\lambda z - 1) - \sinh\lambda z + \frac{\lambda}{2l}(2zl - z^2)\right] \tag{70}$$

It is to be noted that the influence of direct transverse shear is neglected in the bending slope relations (66) and (69).

In order to evaluate the influence of constrained warping on the torsional behavior of these beams, torsional stiffness is determined as the applied tip torsion per unit tip twist from Eq. (65):

$$\text{Torsional stiffness (TS)} = \frac{\lambda(K_{55})_r}{\mu - 2\tanh(\mu/2)} \tag{71}$$

Torsional stiffness corresponding to free warping torsion is obtained from relation (61):

$$(\text{TS})_s = \frac{(K_{55})_r}{l} \tag{72}$$

It is convenient to represent the total torsional stiffness as relative torsional stiffness (RTS) with respect to free warping torsional stiffness.

$$\text{RTS} = \frac{\mu}{\mu - 2\tanh(\mu/2)} \tag{73}$$

It is interesting to note that the relative torsional stiffness is controlled by an important parameter μ. The μ as defined by Eq. (67) depends upon the coefficients of stiffness matrix and length of I-beam. Thus, the influence of geometry and material on the torsional behavior of the I-beam is felt through this parameter.

In order to examine the bending-torsion behavior of these beams in the absence of constrained warping effects, the bending slope and induced twist of a symmetric I-beam subjected to a tip bending load are obtained using relations (57) and (59):

$$\phi_y = -\frac{P}{2(K_{22})_r}(z^2 - 2lz) \tag{74}$$

$$\phi_z = -\frac{K_{25}}{K_{55}}\frac{P}{2(K_{22})_r}(z^2 - 2lz) \tag{75}$$

where $(K_{22})_r = K_{22} - (K_{25}^2/K_{55})$.

Relative induced twist defined as the ratio of induced twist to bending slope at tip is

$$\text{Relative induced twist} = K_{25}/K_{55} \tag{76}$$

Symmetric I-Beams Under Extensional Loads

Extensional load is

$$N = \overline{N}, \qquad G_x = G_y = 0 \tag{77}$$

Inverting relation (50) and integrating with respect to z gives

$$W = \frac{\overline{N}}{\overline{K}_{11}} z \tag{78}$$

where

$$\overline{K}_{11} = K_{11}\left[1 - \frac{K_{16}^2}{K_{11}K_{66}} - \frac{K_{17}^2}{K_{11}K_{77}}\right] \tag{79}$$

Extensional stiffness (ES), which is defined as the load per unit tip extension, is computed from relation (78):

$$\text{ES} = \overline{K}_{11}/l \tag{80}$$

Extensional stiffness is represented as relative extensional stiffness (RES) with respect to the extensional stiffness without transverse shear:

$$\text{RES} = \left[1 - \frac{K_{16}^2}{K_{11}K_{66}} - \frac{K_{17}^2}{K_{11}K_{77}}\right] \tag{81}$$

Experiment

In order to validate the analysis, bending-torsion coupled composite I-beams were built by employing an autoclave molding technique. Figure 2 shows the details of fabrication of beam specimens. Graphite-epoxy or Kevlar-epoxy prepeg layers were laid up on a metal mold which consisted of two parts. Each of these parts would yield beams of channel section. For the fabrication of I-section beams, each part of the mold was wrapped with the desired number of prepeg layers. These layers were compacted by applying vacuum between the mold and lay-up. The two parts of the mold were placed back to back and additional layers were introduced on the top and bottom flanges. Peel ply was wrapped to provide the surface finish of the beam. In order to bleed out excess resin and to permit the escape of volatiles during the curing process, a number of bleeder and breather layers were then applied.

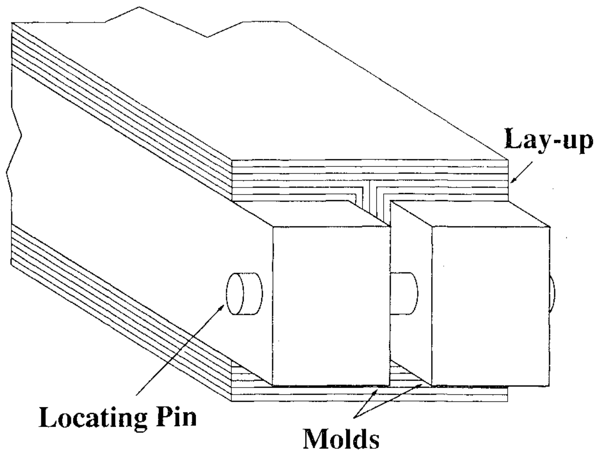

Fig. 2 Fabrication of a composite I-beam.

The lay-up was cured in a microprocessor-controlled autoclave as per the curing cycle given by the manufacturer. At the end of the cure cycle, the lay-up was removed from the autoclave, and then the vacuum bag, bleeder, breather, and release plies were removed, and the beam was released from the mold. Thus composite I-beams with a length of 36 in. and three different slenderness ratios were built.

Table 1 shows the details of I-beams involving five different configurations. These beams are symmetric with respect to midplane; the beams with the angle plies in the flanges have bending-torsion coupling. These I-beams were tested for their static structural response under tip bending and tip torsion loadings separately. A simple test setup,[3] where loads were applied by means of pulleys and dead weight, was used for these tests. In order to avoid buckling of the web while clamping, the web was reinforced with stiff plates and five bolts (Fig. 3). At the loading end, a special fixture was used to ensure that the bending load passes through the shear center. Warping displacements at the clamped and loading ends were constrained in this test setup. The structural response was measured in terms of bending slope and elastic twist at different spanwise stations. These were determined by measuring the rotations of 0.165-in.-diam mirrors in two orthogonal planes, surface-mounted along the span of the test beams. A 2-mW helium-neon laser was used as a light source for this setup.

Results and Discussion

The present analysis is validated with measured results keeping in view three important aspects of open-section beam theory. These are constrained warping effects, slenderness ratio, and fiber orientation and stacking of plies of beam. The slenderness ratio is defined as the ratio of effective length to height of the beam.

The variation of relative torsional stiffness in terms of Saint Venant torsion for a cantilevered I-beam subjected to tip torsional load is illustrated in Fig. 4 for different values of μ. It is seen from this figure that the relative torsional stiffness decreases with an increase in μ, and reaches an asymptotic value of 1, which refers to free warping torsion case. The parameter μ determines the influence of constrained warping on torsional stiffness of the beam, and is a function of cross-sectional stiffnesses and length. It is to be noted that the influence of constrained warping effects on relative torsional stiffness becomes very significant for low value of μ. For a large value of μ (larger than 40), the effect of constrained warping on torsional stiffness is negligible and hence its behavior is controlled by Saint Venant torsion. For a 0/90 CRP I-beam with slenderness ratio of 15 (CRP1), the relative torsional stiffness is 83, whereas this value for a 0/90 CRP I-beam with slenderness of 30 (CRP2) is 6.37. The influence

Table 1 Details of thin-walled composite I-beams

Cases	Width and height, in.	Flanges Top	Flanges Bottom	Web
CRP1	2 × 2	$[0/90]_4$	$[0/90]_4$	$[0/90]_4$
CRP2	1 × 1	$[0/90]_4$	$[0/90]_4$	$[0/90]_4$
CRP3	1 × 0.5	$[0/90]_4$	$[0/90]_4$	$[0/90]_4$
CRP4	1 × 0.5	$[0/90]_3/[15]_2$	$[0/90]_3/[15]_2$	$[0/90]_4$
CRP5	1 × 0.5	$[0/90]_3/[30]_2$	$[0/90]_3/[30]_2$	$[0/90]_4$

Length = 36 in.; number of layers = 8. Carbon reinforced plastic (CRP) I-beam: E_1 = 20.59 × 10^6 psi, E_2 = 1.42 × 10^6 psi, G_{12} = 0.89 × 10^6 psi, μ_{12} = 0.42. Ply thickness = 0.005 in.; wall thickness = 0.04 in.

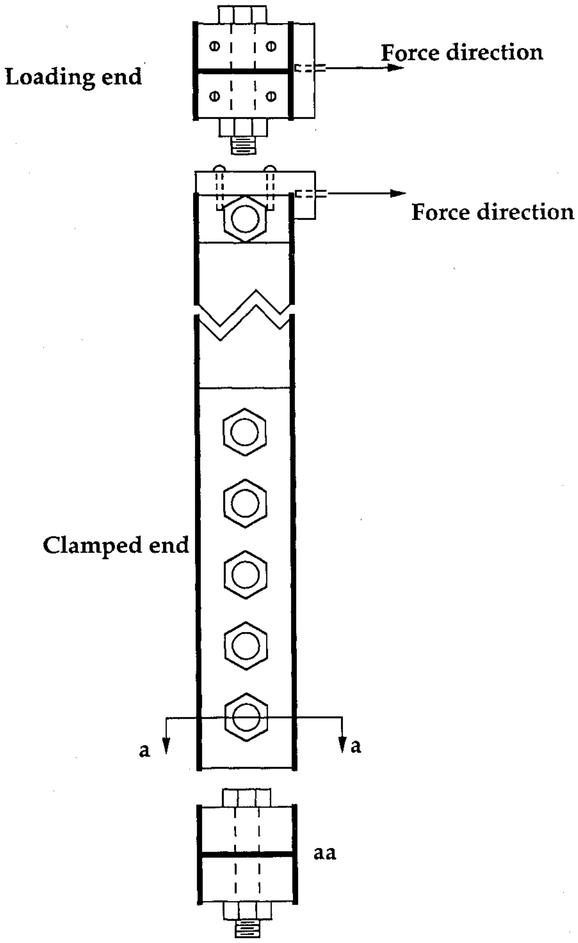

Fig. 3 Details of clamped and loading ends of I-beam.

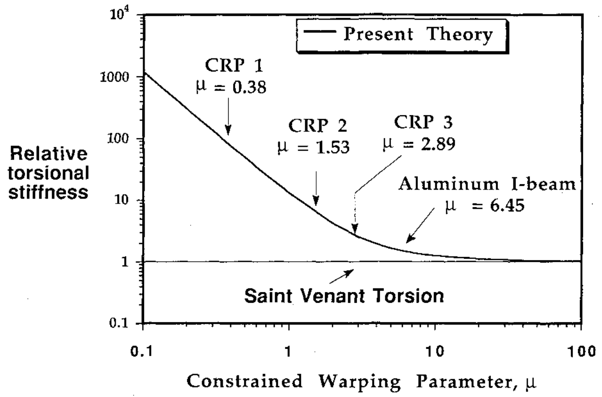

Fig. 4 Variation of relative torsional stiffness of I-beams with constrained warping parameter.

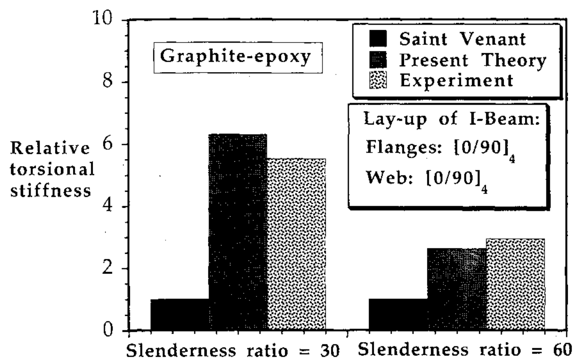

Fig. 5 Torsional stiffness of symmetric graphite-epoxy I-beams under tip torsional load.

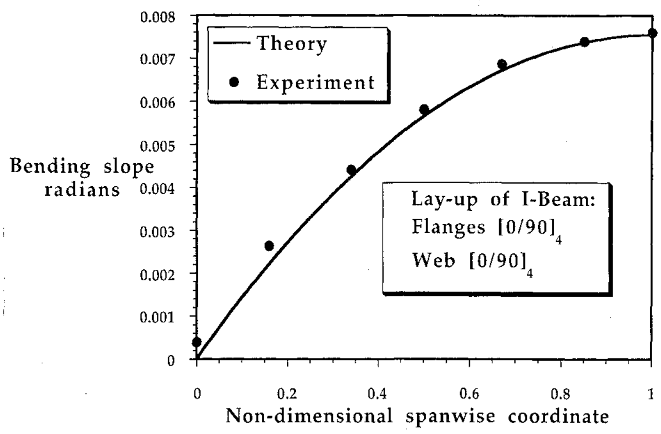

Fig. 6 Variation of bending slope in symmetric graphite-epoxy I-beam (CRP3) under unit tip bending load.

of composite material on relative torsional stiffness is illustrated by comparing the results for a 0/90 CRP I-beam with slenderness ratio of 60 (CRP3) and for an identical aluminum I-beam. It is to be noted that the value of relative torsional stiffness for a CRP3 I-beam is 2.62, whereas for an aluminum I-beam, this value becomes 1.52. This shows that the effect of constrained warping on torsional stiffness is smaller for isotropic materials than for composites. Figure 5 illustrates the effect of constrained warping on the theoretical and experimental values of relative torsional stiffnesses of 0/90 CRP I-beams for two slenderness ratios. A good correlation between theory and experiment is seen only when constrained warping is included in the analysis. The effect of constrained warping on torsional stiffness is very substantial and becomes larger for smaller slenderness ratios.

Figure 6 represents the distributed bending slope of a 0/90 symmetric graphite-epoxy I-beam of slenderness ratio 60 (CRP3) subjected to a unit tip bending load. Figure 7 shows the twist distribution of this beam subjected to unit tip torsional load. This beam has no bending-torsion coupling. Very good correlation between theory and experiment is noticed from these figures. It is to be noted from Figs. 6 and 7 that this beam is many times softer in torsion as compared to bending. The ratio of torsional flexibility (tip twist per unit torsional load) to bending flexibility (tip bending slope per unit bending load) is about 35. This is not surprising for an open cross section such as I-beam.

Figure 8 shows the bending slope and induced twist of a symmetric graphite-epoxy 15-deg I-beam (CRP4) subjected to a unit tip bending load. This beam results in bending-torsion and extension-shear couplings. A very good correlation between theory and experiment is achieved for this beam. Also, it is to be noted that the induced twist is about four times the bending slope for this beam under bending load. Figure 9 shows the spanwise variation of twist of this beam

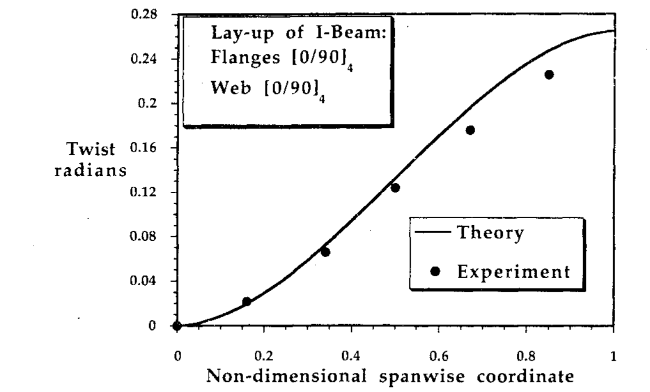

Fig. 7 Variation of twist in symmetric graphite-epoxy I-beam (CRP3) under unit tip torsional load.

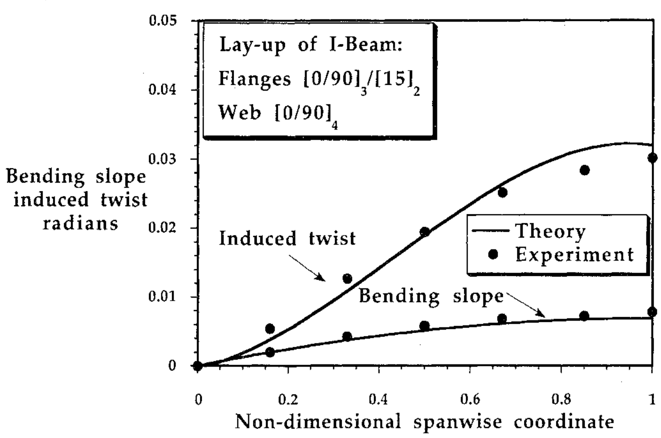

Fig. 8 Variation of bending slope and induced twist in symmetric graphite-epoxy I-beam (CRP4) under unit tip bending load.

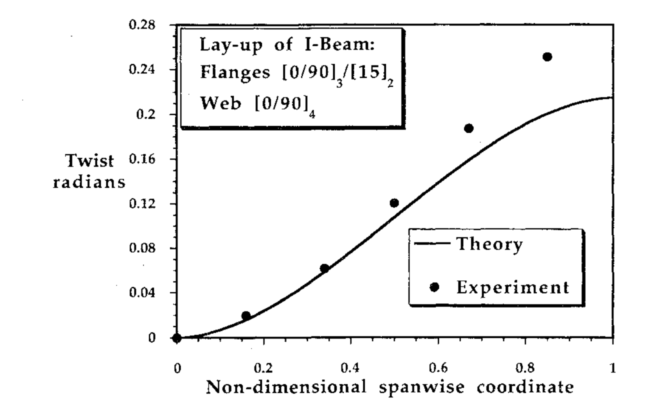

Fig. 9 Variation of twist in symmetric graphite-epoxy I-beam (CRP4) under unit tip torsional load.

under a unit tip torsional load. Correlation between theory and experiment is generally satisfactory except near the tip. The torsion induced-bending slope for this beam is too small and therefore is not represented in this figure.

The bending slope and induced twist of a symmetric 30-deg graphite-epoxy I-beam (CRP5) subjected to a unit tip bending load are presented in Fig. 10. Very good correlation between theory and experiment is seen in this figure. The induced twist is about five times the bending slope for this beam under bending load. Figure 11 shows the twist variation along the span of this beam under a unit tip torsional load. Good correlation between theory and experiment is noticed for this beam.

As seen from relation (A2), the bending-torsion coupling stiffness K_{25} for composite I-beams depends upon B_{16} and D_{16} stiffness coefficients of flanges. B_{16} refers to extension-twist coupling and D_{16} refers to bending-twist coupling of the plate segment of the I-beam. It is possible to select the flanges such that B_{16} is zero; meaning that the flanges are symmetric with respect to their own mid surfaces. It is interesting to examine the sensitivity of bending-torsion coupling K_{25} to B_{16} and D_{16}. The 15-deg symmetric graphite-epoxy I-beams discussed earlier are made out of flanges that are not symmetric with respect to their own midplanes. Hence B_{16} for these beams is nonzero. Figure 12 shows the influence of B_{16} on bending slope and induced twist of these beams subjected to a unit tip bending load. For comparison purposes, the results are given for beams with $B_{16} = 0$. It is interesting to note that for these beams, it is B_{16} that produces the bending-torsion coupling in I-beams. The contribution of D_{16} is too small to be presented in this figure.

Figure 13 shows the influence of constrained warping effects on the relative induced twist with respect to the bending slope, of various I-beams subjected to tip bending loading. It is interesting to note that the constrained warping reduces the induced twist via increase in torsional stiffness.

Figure 14 shows the influence of transverse shear deformation on extensional stiffnesses of graphite-epoxy I-beams (CRP4 and CRP5). It is to be noted from this figure that the transverse shear, through extension-shear coupling, reduces the extensional stiffness of the beam; the amount of reduction depends upon the lay-up of beam. About a 10% reduction in extensional stiffness is seen for a 30-deg I-beam (CRP5).

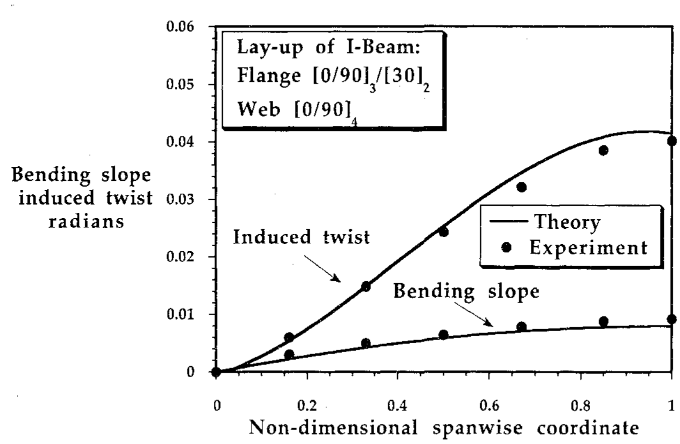

Fig. 10 Variation of bending slope and induced twist in symmetric graphite-epoxy I-beam (CRP5) under unit tip bending load.

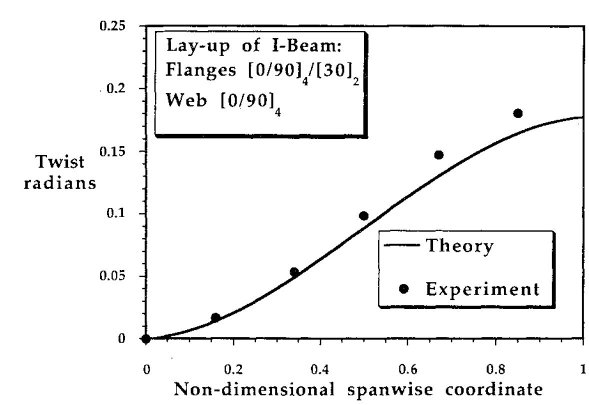

Fig. 11 Variation of twist in symmetric graphite-epoxy I-beam (CRP5) under unit tip torsional load.

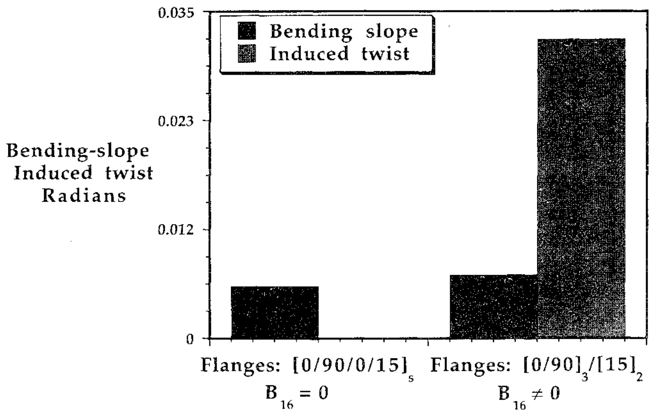

Fig. 12 Influence of extension-twist coupling stiffness of flanges of symmetric graphite-epoxy I-beam on its induced twist under tip bending load.

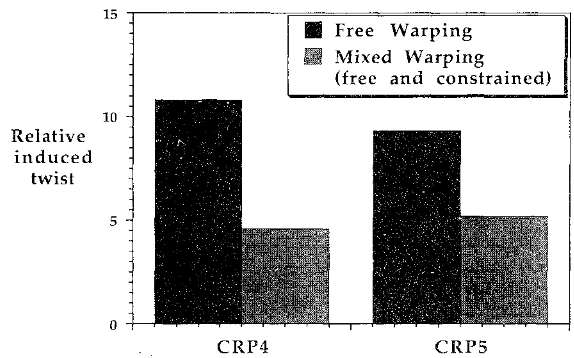

Fig. 13 Influence of constrained warping on relative induced twist of I-beam subjected to tip bending load.

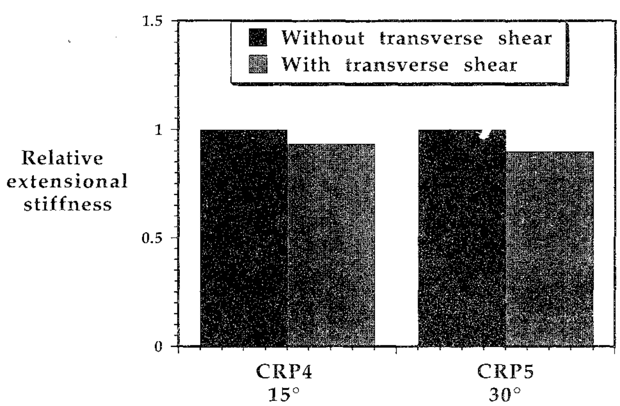

Fig. 14 Influence of transverse shear deformation on relative extensional stiffness of I-beams under extensional load.

Conclusion

Vlasov's theory is expanded to perform the linear analysis of open-section I-beams made out of general composite laminates. Transverse shear deformation of the beams is accounted for in the theory. In order to provide experimental correlation to the theory, graphite-epoxy I-beams covering various parameters, such as fiber orientation and stacking sequence of plies and slenderness ratios, were fabricated using an autoclave molding technique. These beams were tested for their structural response under tip bending and torsional loads, and bending slope and twist were measured along the length of the beam. Very good correlation between theory and experiment was achieved. Based on this study, the following conclusions are made:

1) The torsional stiffness of I-beams is significantly influenced by restraining the warping deformations of the beam. About a 260–640% increase in torsional stiffness because of constrained warping was seen for the graphite-epoxy beams.

2) The structural behavior of I-beams with bending-torsion coupling is also influenced substantially by constraining the warping deformations of the beam. Relative induced twist with respect to bending slope at tip is reduced by about 40% by constrained warping.

3) The bending-torsion coupled behavior of I-beams is influenced by bending-twist and extension-twist couplings of its plate segments. Extension-twist coupling of plate segments increases the bending induced twist for the beams examined by about 460–520%.

4) Slenderness ratio controls the influence of warping constrained effects on torsional stiffness. Constrained warping effects enhances the torsional stiffness of shorter beams more than for slender ones.

5) Transverse shear deformation has a negligible influence on the structural behavior of symmetric I-beams under bending and torsional loads.

Appendix: Stiffness Matrix K of I-Beam

$$K_{22} = 2b[D_{11}^{(b)} + D_{11}^{(t)}] + 2bh^2[A_{11}^{(b)} + A_{11}^{(t)}] + \frac{2h^3}{3} A_{11}^{(w)} \tag{A1}$$

$$K_{25} = 4b[D_{16}^{(b)} - D_{16}^{(t)}] + 4bh[B_{16}^{(b)} - B_{16}^{(t)}] \tag{A2}$$

$$K_{44} = \frac{2b_3}{3}[h^2(A_{11}^{(b)} + A_{11}^{(t)}) + D_{11}^{(b)} + D_{11}^{(t)}] + \frac{2h^3}{3} D_{11}^{(w)} \tag{A3}$$

$$K_{55} = 4b[D_{66}^{(b)} + D_{66}^{(t)}] + 4hD_{66}^{(w)} \tag{A4}$$

$$K_{11} = 2b[A_{11}^{(b)} + A_{11}^{(t)}] + 2hA_{11}^{(w)} \tag{A5}$$

$$K_{16} = 2b[A_{16}^{(b)} - A_{16}^{(t)}] \tag{A6}$$

$$K_{17} = 2hA_{16}^{(w)} \tag{A7}$$

$$K_{66} = 2b[A_{66}^{(b)} + A_{16}^{(t)}] \tag{A8}$$

$$K_{77} = 2hA_{66}^{(w)} \tag{A9}$$

$$A_{ij} = \sum_{k=1}^{\#\text{ of layers}} Q_{ij}^{(k)}(h_{k+1} - h_k) \tag{A10}$$

$$B_{ij} = \frac{1}{2} \sum_{k=1}^{\#\text{ of layers}} Q_{ij}^{(k)}(h_{k+1}^2 - h_k^2) \tag{A11}$$

$$D_{ij} = \frac{1}{3} \sum_{k=1}^{\#\text{ of layers}} Q_{ij}^{(k)}(h_{k+1}^3 - h_k^3) \tag{A12}$$

$Q_{ij}^{(k)}$ refers to stiffness matrix of kth layer or web in sz plane. h_{k+1} and h_k are coordinates of kth layer in n direction from midplane of laminates as reference surface.

Acknowledgments

This research work has been supported by the Army Research Office under Contract DAAL-03-88-C022, Technical Monitors, Robert Singleton, and Tom Doligalski.

References

[1]Hong, C. H., and Chopra, I., "Aeroelastic Stability of a Composite Blade," *Journal of the American Helicopter Society*, Vol. 30, No. 2, 1985, pp. 57–67.

[2]Panda, B., and Chopra, I., "Dynamics of Composite Rotor Blades in Forward Flight," *Vertica*, Vol. 11, No. 1/2, 1987, pp. 187–209.

[3]Chandra, R., Stemple, A. D., and Chopra, I., "Thin-Walled Composite Beams under Bending, Torsional and Extensional Loads," *Journal of Aircraft*, Vol. 27, No. 2, 1990, pp. 619–627.

[4]Smith, E. C., and Chopra, I., "Formulation and Evaluation of an Analytical Model for Composite Box Beams," *Proceedings of the 31st AIAA/ASME/ASCE/AHS/ASC Structures, Structural Dynamics and Materials Conference*, AIAA, Washington, DC, April 1990.

[5]Chandra, R., and Chopra, I., "Influence of Elastic Couplings on Vibration Characteristics of Thin-Walled Box Beams under Rotation," *Journal of Aircraft* (to be published).

[6]Rehfield, L. W., Atilgan, A. R., and Hodges, D. H., "Nonclassical Behavior of Thin-Walled Composite Beams with Closed Cross Sections," *Journal of the American Helicopter Society*, Vol. 35, No. 2, 1990, pp. 42–50.

[7]Bauchau, O. A., "A Beam Theory for Anisotropic Materials," *Transactions of the American Society of Mechanical Engineers, Journal of Applied Mechanics*, Vol. 52, June 1985, pp. 416–422.

[8]Kosmatka, J. B., "Extension, Bending and Torsion of Anisotropic Beams with Initial Twist," *Proceedings of the 30th AIAA/ASME/ASCE/ASC Structures, Structural Dynamics and Materials Conference*, AIAA, Washington, DC, April 1989.

[9]Minguet, P., and Dugundji, J., "Experiments and Analysis for Composite Blades Under Large Deflections: Part 1. Static Behavior," *AIAA Journal*, Vol. 28, No. 9, 1990, pp. 1573–1579.

[10]Stemple, A. D., and Lee, S. W., "A Finite Element Model for Composite Beams with Arbitrary Cross Sectional Warping," *AIAA Journal*, Vol. 26, No. 12, 1988, pp. 1512–1520.

[11]Kosmatka, J. B., and Friedmann, P. P., "Structural Dynamic Modeling of Advanced Composite Propellers by the Finite Element Method," *Proceedings of the 28th AIAA/ASME/ASCE/ASC Structures, Structural Dynamics and Materials Conference*, AIAA, Washington, DC, April 1989.

[12]Bauchau, O. A., and Hong, C. H., "Finite Element Approach to Rotor Blade Modeling," *Journal of the American Helicopter Society*, Vol. 32, No. 1, 1987, pp. 60–67.

[13]Hong, C. H., and Chopra, I., "Aeroelastic Stability Analysis of a Composite Bearingless Rotor Blade," *Journal of the American Helicopter Society*, Vol. 31, No. 4, 1986, pp. 29–35.

[14]Rehfield, L. W., and Atilgan, A. R., "On the Buckling Behavior of Thin Walled Laminated Composite Open Section Beams," *Proceedings of the 30th AIAA/ASME/ASCE/AHS/ASC Structures, Structural Dynamics and Materials Conference*, AIAA, Washingon, DC, April 1989.

[15]Vlasov, V. Z., *Thin-Walled Elastic Beams*, translated from Russian, 1961, National Science Foundation and Department of Commerce, USA, 1961.

[16]Gjelsvik, A., *The Theory of Thin-Walled Bars*, Wiley, New York, 1981.

[17]Bauld, N. R., Jr., and Tzeng, L. S., "A Vlasov Theory for Fiber Reinforced Beams with Thin-Walled Open Cross-Sections," *International Journal of Solids and Structures*, Vol. 20, No. 3, 1984, pp. 277–297.

[18]Chandra, R., and Chopra, I., "Experimental and Theoretical Analysis of Composite I-beams with Elastic Couplings," *Proceedings of the 32nd AIAA/ASME/ASCE/AHS/ASC Structures, Structural Dynamics and Materials Conference*, AIAA, Washington, DC, April 1991.